MATERIALS CHEMISTRY FRONTIERS

RESEARCH ARTICLE

View Article Online
View Journal | View Issue

Cite this: *Mater. Chem. Front.*, 2024, **8**, 2149

Large-area arrays of epitaxially aligned silver nanotriangles seeded by gold nanostructures†

Zachary R. Lawson,[a] Kaikui Xu,[a] Christina Boukouvala,[cd] Robert A. Hughes,[a] Matthew R. Rosenberger,[a] Emilie Ringe [cd] and Svetlana Neretina *[ab]

Received 6th November 2023,
Accepted 1st February 2024

DOI: 10.1039/d3qm01184d

rsc.li/frontiers-materials

The ability to separate nucleation and growth processes into distinct steps has proved invaluable in achieving high-level control over colloidal synthesis. The success of these so-called seed-mediated pathways has been contingent upon the advancement of synthetic protocols specifically designed to take advantage of the internal defect structures within an otherwise crystalline seed. Noble metal nanoplates represent the most prominent example as their synthesis requires seeds lined with symmetry breaking stacking fault defects that, when placed in a suitably chosen chemical environment, promote two-dimensional heterogeneous deposition. Even though such syntheses are now commonplace, the growth of flat-lying silver nanoplates in arrayed configurations directly on substrate surfaces has heretofore proved unrealizable due to an inability to form appropriately designed seeds in organized patterns. Herein, a silver nanotriangle synthesis is demonstrated on substrate surfaces populated with gold seeds arranged in periodic arrays. Crucial to this success is the relaying of crystallographic information from the substrate to the gold seed to the silver nanotriangle *via* heteroepitaxy. The so-formed nanotriangles exhibit a tunable plasmon resonance where simulations indicate that the response is dominated by the silver component. The work, hence, adds silver nanotriangles to an ever-expanding list of rationally designed nanostructures accessible through substrate-based syntheses.

Introduction

Nanostructure shape control is one of the main tenets of nanoscience and nanotechnology.[1,2] Plasmonic materials represent an exemplary illustration as there now exists an architecturally diverse library of structures with shape-dependent properties that are augmented by variations to their size, composition, and orientation relative to the polarization direction of the incident electromagnetic radiation. Among these, nanostructures exhibiting a two-dimensional planar morphology have attracted widespread interest in terms of the properties they express, the applications forwarded, and the underlying mechanisms that lead to the emergence of a thermodynamically unfavorable geometry with a high surface energy.[3–7] Within this classification, triangular nanoplates stand out as the most prominent planar structure due to (i) a size-dependent localized surface plasmon resonance (LSPR) that extends from visible wavelengths into the infrared,[8] (ii) atomically flat (111) surfaces suitable for precise functionalization,[9] and (iii) large localized electric field enhancements occurring at their sharp tips or between two nanotriangles arranged in a bowtie configuration.[10] In this regard, Ag nanotriangles are far superior to those composed of more lossy metals such as Au and Cu.[11] As such, they are one of the most often synthesized, studied, and utilized plasmonic nanomaterials.[3,4,12]

The mechanistic requirements for Ag nanoplate synthesis center around the establishment of symmetry breaking controls able to steer growth along a two-dimensional pathway even though it is contrary to the centrosymmetric nature of its face-centered cubic (fcc) crystal structure.[3–6] It is widely accepted that symmetry breaking is facilitated by the emergence of stacking faults in the seed formation process.[13–15] These stacking faults, which are disruptions to the stacking order along a ⟨111⟩-axis, break the ABCABC… fcc stacking sequence by adding or subtracting a layer or through an abrupt reversal in the stacking order (*i.e.*, a twin defect). If single or multiple defects occur along just one of the ⟨111⟩-equivalent axes, then it imparts a two-dimensional character upon an otherwise isotropic seed by having stacking fault defects protrude from the seed surface in parallel ring-like patterns. Such defects give rise to convex and concave surface features

[a] *College of Engineering, University of Notre Dame, Notre Dame, Indiana 46556, USA. E-mail: sneretina@nd.edu*
[b] *Department of Chemistry and Biochemistry, University of Notre Dame, Notre Dame, Indiana 46556, USA*
[c] *Department of Materials Science and Metallurgy, University of Cambridge, Cambridge CB30FS, UK*
[d] *Department of Earth Sciences, University of Cambridge, Cambridge CB23EQ, UK*
† Electronic supplementary information (ESI) available. See DOI: https://doi.org/10.1039/d3qm01184d

where the resulting reentrant grooves are conducive to the reduction of Ag^+ ions.[13,16] The mere existence of stacking faults is, however, insufficient in realizing high aspect ratio planar geometries[17] but must instead be complemented by a nanoplate growth solution containing a suitably chosen (111) capping agent. This agent has multiple roles in that it must (i) prevent the reduction of Ag^+ ions directly onto the top and bottom surfaces of the nanoplate, (ii) block the diffusion of deposited Ag atoms from the edges to the planar surfaces, (iii) show a limited tendency toward the capping of the active growth sites on the periphery of the nanoplate, and (iv) provide colloidal stability. With these crucial elements in place, the nanoplate grows laterally as the depositing atoms replicate the defects needed to sustain the two-dimensional growth mode.

The Mirkin group demonstrated the first synthetic protocol able to generate a colloid of crystalline Ag nanotriangles.[18] This landmark discovery generated an intense interest that has since given rise to an expansive literature that includes a wide variety of approaches directed toward the realization of nanoplates with a triangular geometry. Even though these methodologies vary considerably, they are united by commonalities that include a need for (i) seeds with the required stacking fault defects, (ii) a source of Ag^+ ions, (iii) a reductant, and (iv) a capping agent. Seed preparation techniques typically take advantage of the increased stability of seeds with stacking fault defects when placed in chemical environments where less stable seeds are eliminated through etching processes reliant on H_2O_2[19,20] or dissolved oxygen.[18,21,22] Single-step syntheses typically use the ions released in this seed purification process as the source of Ag[18,19,21,22] while two-step seed-mediated syntheses rely on $AgNO_3$[14,23] or CF_3COOAg.[17] The means by which Ag^+ ions are reduced is dependent upon whether the nanotriangle growth mode is driven by plasmonic excitations,[21] a reducing agent,[17,24,25] or a combination of the two,[19] where citrate is typically used for the former while sodium borohydride,[19,24] polyvinylpyrrolidone (PVP),[25,26] and ascorbic acid (AA)[14,17,23] have all proven effective for the latter. Citrate is by far the most commonly used capping agent where its selective passivation is attributed to a close geometric match between its three carboxylic acid groups and the hexagonal close-packed (111) surface of Ag.[17,27,28] It is, however, noted that other carboxyl compounds,[29] as well as PVP,[25,26] have also given rise to triangular nanoplates. Another reagent of note is acetonitrile which has been included in some protocols for its ability to form complexes with Ag^+ ions, and in doing so, can slow reaction rates to lessen the number of seeds formed in the nucleation step[30] or inhibit the spontaneous nucleation of Ag nanostructures in seed-mediated growth modes.[23] Altogether, these various colloidal syntheses represent an impressive collection that has led to the establishment of Ag nanotriangles as a renowned nanoscale building block where capabilities in terms of scalability,[23,31] yield,[23,24] and control over nanotriangle dimensions[21,23,32] are all well-documented.

When compared to the unmitigated successes associated with the colloidal synthesis of Ag nanotriangles, efforts directed toward synthesizing similar structures directly on substrate surfaces appear somewhat subdued. These efforts have largely centered around three strategies: (i) the adhesion of colloidal seeds to a functionalized substrate surface followed by its exposure to a liquid-state chemical environment conducive to nanoplate formation,[33–38] (ii) electrochemical syntheses that form nanoplates directly on an electrode surface,[39–43] and (iii) through the exposure of a synthetically active substrate to aqueous $AgNO_3$ where chemical reactions involving the substrate material allow the synthesis to proceed.[44–47] These methodologies are, however, less than optimal in that the majority have resulted in the formation of disorganized networks of nanoplates where size and shape uniformity is absent and where the nanoplates, more often than not, have a growth trajectory that is away from the substrate surface. Even though nanoplates are produced in high yield, the nanotriangle geometry has only rarely been observed[35,44] and the deterministic placement of individual structures on the substrate surface has not yet been achieved. With a recent resurgence in interest in the integration of single-crystal nanometals with wafer-based techniques,[4,48–56] addressing these unmet challenges in nanometal synthesis becomes a priority. Herein, a four-reagent seed-mediated synthesis is demonstrated that gives rise to Ag nanotriangles at predefined locations using Au seeds arranged in a periodic array. By using Au seeds instead of Ag, it has proved possible to obtain the required stacking fault defects and, in doing so, avoid many of the pitfalls that have limited prior syntheses.

Results

With the deterministic positioning of Ag nanotriangles on substrate surfaces being the underlying goal of this work, it is imperative that their formation proceed along a two-step protocol where seeds with the required defect structures are first formed in periodic arrays followed by their exposure to a liquid-state synthesis that sees them transformed into nanotriangles. As such, seed formation is a critical component where the techniques forwarded in colloidal chemistry are incompatible because controls leading to their proper placement do not exist. Because it is desirable to have the nanotriangle lie flat on the substrate surface so that light directed at normal incidence can excite the in-plane dipole resonance and produce intense near-fields at its corners, it is imperative that seeds are designed that have both their [111]-axis and stacking fault defects appropriately aligned relative to the substrate surface. Fig. 1 illustrates this concept by first showing an idealized freestanding seed, which expresses eight {111} and six {100} facets, onto which red lines are drawn to denote the location where stacking faults would have to exist to make such a seed suitable for nanoplate growth. The seed is then placed on a substrate surface in the eight possible configurations where each of its {111} facets form an interface with the substrate. Even though all of these seed–substrate configurations fulfil the crystallographic requirements for nanotriangle growth, only the first two are capable of realizing nanotriangles that lie flat on the surface while the remainder

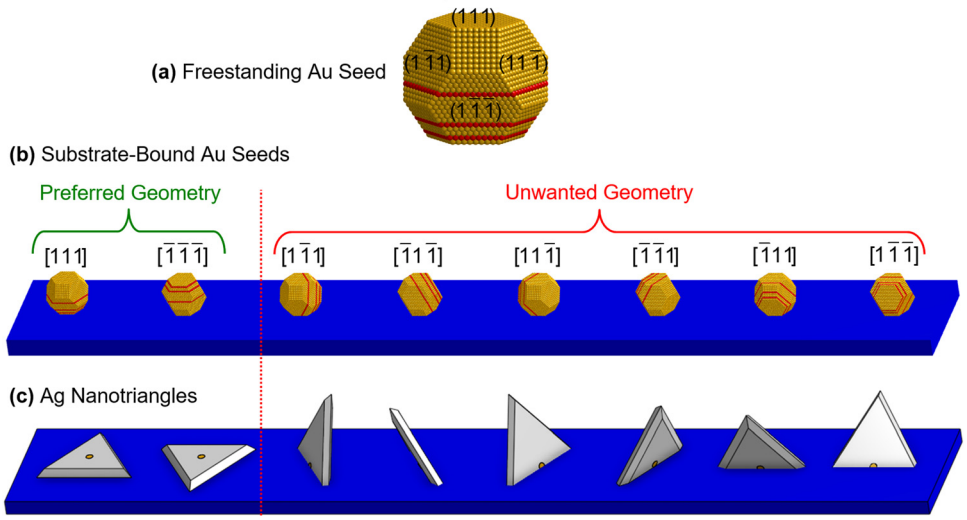

Fig. 1 Schematic illustrating a (a) freestanding truncated octahedron seed where the dashed red lines represent the positions where stacking faults defects would have to be located to achieve a break in symmetry conducive to planar growth modes, (b) the placement of the seed onto a substrate in the eight possible configurations that allow a {111} facet to mate with the surface, and (c) the triangular nanoplates that emerge from each seed.

result in growth trajectories that project out of the substrate surface at 70.53°. It is, therefore, not enough for the seeds to merely have symmetry breaking stacking fault defects along a single ⟨111⟩-direction but must instead have defects with the correct alignment relative to the surface of the substrate if the preferred nanotriangle geometry is to be realized. This is a challenge that is unique to substrate-based nanoplate growth and, to a large degree, is the reason why achieving high-level control over substrate-based Ag nanotriangle growth modes has proved difficult.

In a prior report,[57] we demonstrated a seed fabrication process that yielded periodic arrays of Au nanoplates with the preferred geometry at yields as high as 78% by taking advantage of the heteroepitaxial interactions occurring at the seed–substrate interface during a high-temperature vapor-phase seed assembly process. These interactions allowed the substrate to induce the desired [111] Au seed orientation where stacking fault defects showed a strong propensity for forming along the axis needed to obtain the preferred geometry. Our attempts to replicate this success with similarly formed Ag seeds proved highly unsatisfactory (Fig. S1, ESI†). As such, a Ag nanotriangle synthesis strategy was designed around the use of Au seeds. It was spurred on by the fact that the small lattice mismatch between Au and Ag of only 0.2% makes layer-by-layer

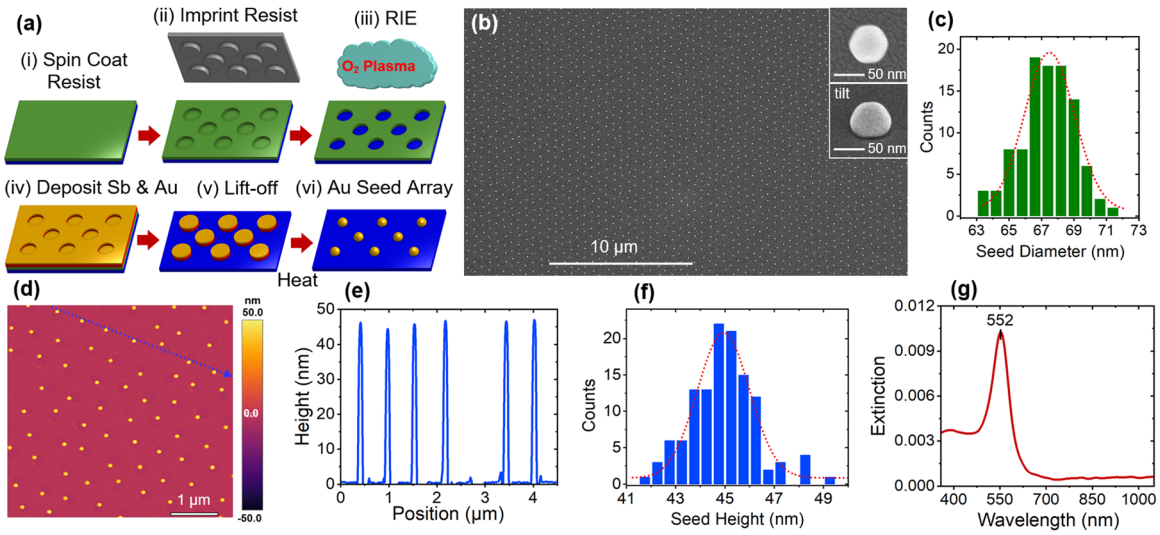

Fig. 2 (a) Schematic of the nanofabrication process used to form a periodic array of Au seeds. (b) SEM image of the array where the insets show an individual structure taken from a top and tilted view. (c) Histogram of the seed diameter extracted from high-resolution SEM images displaying 100 seeds. (d) Topographic AFM image of the seed array from which a (e) line scan was extracted. (f) Histogram of the seed height distribution based on 123 seeds. (g) Extinction spectrum of the Au seeds which displays a narrow plasmon resonance at 552 nm.

deposition favorable[58] and the demonstration of colloidal syntheses that have realized nanoplates with both Au and Ag segments.[59,60]

The nanofabrication process used to form periodic arrays of Au seeds is shown schematically in Fig. 2(a). The process, which is described in detail elsewhere,[57,61] uses nanoimprint lithography in combination with reactive ion etching (RIE) to define cylindrical openings in a moldable polymeric resist that expose the substrate surface in a pattern that replicates the imprinted features. A Au–Sb bilayer is then sputter-deposited over the entire surface followed by a lift-off process that leaves behind an array of Au-topped Sb disks. Upon heating, the polycrystalline Au layer formed at the top of each disk assembles into a crystalline nanostructure lined with stacking faults[57] as the sacrificial Sb layer is lost to sublimation.[62] Crucial to the success of this process is the use of a [0001]-oriented sapphire substrate in that it forms an epitaxial relationship with the (111) surface of Au[63] that induces the required seed orientation and stacking fault defects.[57] Fig. 2(b) shows an SEM image of a seed array where structures are arranged in a hexagonal pattern with a center-to-center distance of 600 nm. The insets to the figure show high-resolution images of a single structure from a top and side view. They reveal the faceting anticipated for a [111]-oriented truncated octahedron that has been further truncated at its base. Truncated octahedrons exhibiting this apparent truncation represent the equilibrium shape for metal nanoparticles supported on a low surface energy substrate.[64,65] Fig. 2(c) shows a histogram of seed diameters derived from an analysis of SEM images that reveals a narrow size distribution centered around 67 nm. Fig. 2(d)–(f) shows AFM characterization in the form of a topographic image, a line scan across six structures, and a seed height histogram, all of which reveal a near-constant height of approximately 45 nm. The sharpness of these seed size distributions also express themselves in a spectral response that is characterized by a rather sharp plasmon resonance centered at 552 nm (Fig. 2(g)). It should,

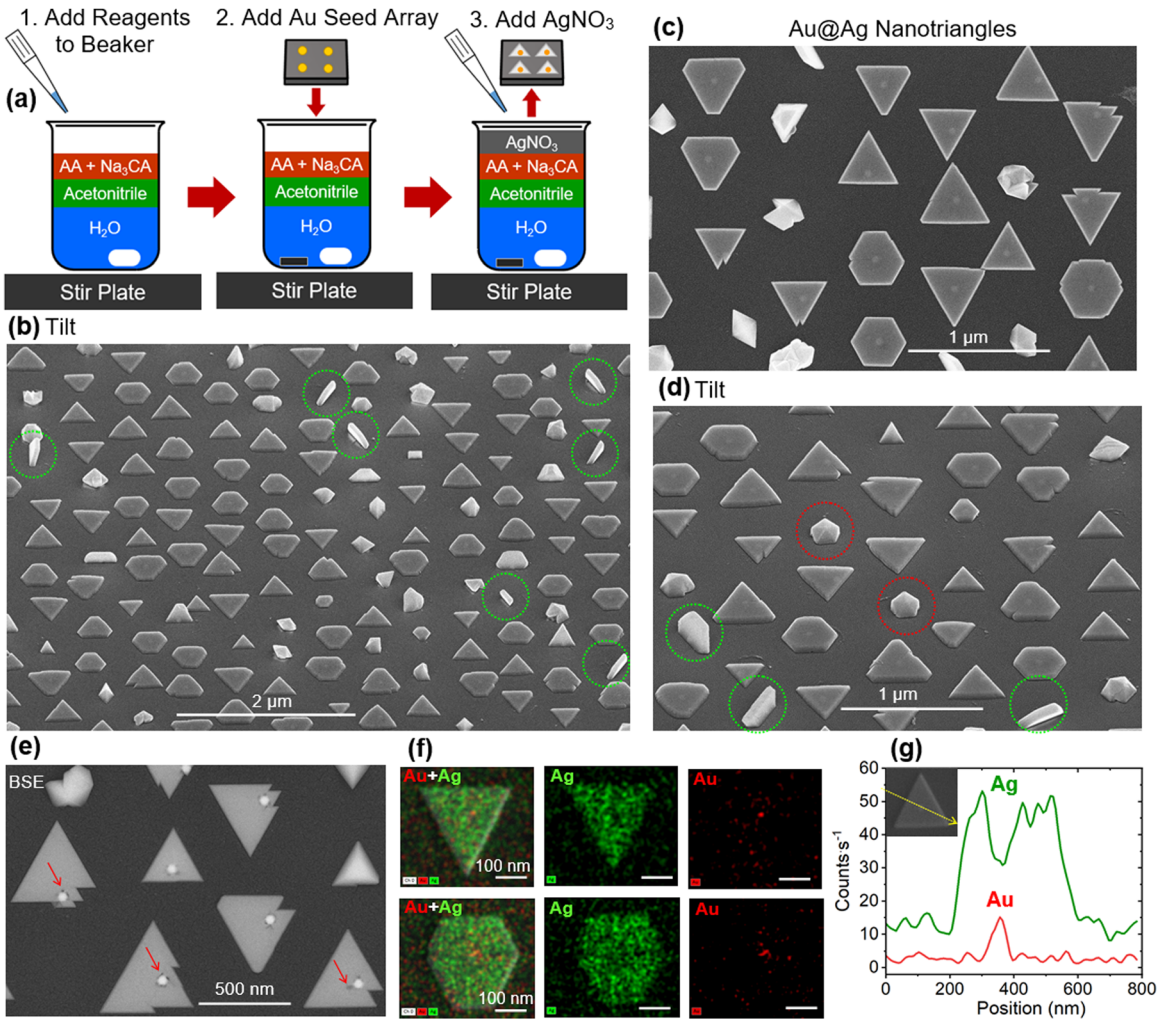

Fig. 3 (a) Schematic illustrating the procedure used for Ag nanotriangle synthesis. (b) Low-magnification tilted-view SEM image of the synthesized structures. (c) Top- and (d) tilted-view SEM images taken at a higher magnification. (e) BSE SEM image revealing the location of the Au seeds. (f) Elemental mapping of a triangular and hexagonal nanoplate with a centrally located seed. (g) Elemental line scan derived from energy-dispersive spectroscopy (EDS) taken along a trajectory that passes through the Au seed.

however, be noted that the seed size varies slightly from sample-to-sample due to the idiosyncrasies of imprinting, deposition, and assembly processes.

In an ideal scenario, the design of a substrate-based Ag nanotriangle synthesis would see the adoption of an existing seed-mediated colloidal chemistry protocol where the only major difference is that the solution dispersed seeds are substituted for a substrate-bound array of similarly configured seeds. Most of the existing syntheses were, however, deemed unsuitable. Syntheses where nanotriangle formation was contingent upon the formation of population of sacrificial Ag nanostructures whose disintegration through etching processes provides a Ag^+ feedstock for growing nanotriangles were ruled out because they pose the risk of having these spontaneously formed colloidal structures adhere to the substrate, an occurrence that has proved problematic in other substrate-based syntheses.[66] This narrowed the search to a rather small subset of syntheses[14,17,23] designed to inhibit the spontaneous nucleation of Ag nanostructures as heterogeneous growth proceeded onto preformed nanoplates that acted as seeds. The syntheses carried out in the current study were, hence, adapted from the protocol of Gao and co-workers[23] who formed populations of uniformly sized nanotriangles with edge lengths ranging from 150 nm to 1.5 μm using triangular seeds with widths and edge lengths of 5 and 30 nm, respectively. The protocol sees seeds injected into a 5 °C aqueous solution of $AgNO_3$, AA, trisodium citrate (Na_3CA), and acetonitrile where these reagents act as the metal precursor, reducing agent, capping agent, and coordinating ligand for the Ag^+ ions, respectively. The inclusion of acetonitrile is of specific importance because its complexation significantly decreases the reduction potential of Ag,[23] an outcome that severely inhibits unwanted homogeneous nucleation and slows the rate of heterogeneous deposition onto the seeds. As such, the nanotriangles grow in a kinetically controlled regime.

Fig. 3(a) presents a schematic illustrating the synthetic procedure used to form substrate-based Ag nanotriangles. It begins with the preparation of a beaker containing an aqueous solution of AA, Na_3CA, and acetonitrile where magnetic stirring ensures that the reagents are sufficiently mixed. A Au seed array is then immersed into the solution such that it lies faceup at the bottom of the beaker adjacent to a Teflon stir bar. The reaction is initiated through the injection of $AgNO_3$ and allowed to proceed for 20 min, after which it is terminated through the removal of the substrate from the growth solution. With the substrate-based seeds being the only sites for heterogeneous nucleation, the growth solution remains clear over the course of the reaction. Spectral characterization of the growth solution performed before and after a Ag nanotriangle synthesis reveals near-overlapping featureless spectra (Fig. S2, ESI†). These observations indicate that acetonitrile is effective in suppressing homogeneous nucleation, a conclusion that is verified by the formation of an Ag colloid when the reaction is carried out in its absence (Fig. S3, ESI†).

Fig. 3(b)–(d) shows SEM images of the synthesized structures. A large area image as well as a statistical analysis of the product is presented in Fig. S4 and S5 (ESI†), respectively. As anticipated, a large percentage of the structures express the preferred nanoplate geometry where their planar surface lies flat on the substrate. These structures exhibit both triangular and hexagonal geometries where some appear distorted in that they have jagged edges. High-magnification images also reveal that many of these nanoplates exhibit crack-like features that extend from the edge of the Au seed to the perimeter of the Ag nanoplate (Fig. S6, ESI†). A smaller subset of the arrayed structures are nanoplates where the growth trajectory is directed away from the surface of the substrate at a slight tilt from the normal (denoted by green circles in Fig. 3(b) and (d)). The orientation and tilt angle observed are consistent with growth off of Au seeds having stacking fault defects in a direction other than the preferred direction. The remainder of the structures are attributed to defective seeds having a corrupted heteroepitaxial relationship with the substrate, exhibiting multidomains, or which are multiply twinned. Interesting is the formation of pentatwinned structures (denoted by red circles in Fig. 3(d)) given that the Au seeds are produced at high temperature to sizes where pentatwinned configurations are thermodynamically unfavorable.[67] Fig. 3(e)–(g) shows backscattered electron (BSE) SEM images and the associated elemental mapping and line scans for the nanoplates. A line scan for the hexagonal plate is shown in Fig. S7 (ESI†). Given that the Ag and Au components are clearly distinguishable, these results suggest that interdiffusion at the Au–Ag interface is minimal. This is confirmed by spectroscopic measurements in which the plasmon of the Au seed, measured before growth, is found to be identical with that after a nanoplate growth that is followed by the removal of the Ag component with an etchant (Fig. S8, ESI†). The BSE image also shows that the seed location is often offset from the center of the structure. This indicates that lateral growth preferentially proceeds in some directions while being frustrated in others. It is noteworthy that the preferred growth directions tend to support side-faceting consistent with a nanotriangle whereas directions that are frustrated often display a distorted side-faceting with a jaggedness that corrupts the overall nanotriangle geometry. Also of note is that small voids often appear at the perimeter of the Au seed (denoted by red arrows in Fig. 3(e)).

In an effort to better understand the nanotriangle growth mode, a synthesis was carried out where multiple samples were placed in the same growth solution and removed at various time intervals. Fig. 4 shows a progression that is representative of the growth sequence. The early stages of synthesis give rise to Ag deposition that results in the formation of a triangular feature from which thinner plate-like structures emerge at multiple locations (denoted by red arrows). These thinner structures then thicken to the seed diameter as the growth fronts propagate away from the seed as independent segments. Over time, these segments grow and merge, forming crack-like features in the process. Continued growth sees the emergence of faceting that is more reminiscent of a nanotriangle but where imperfections along the perimeter are present. It is noteworthy that this progression differs greatly from substrate-based Au

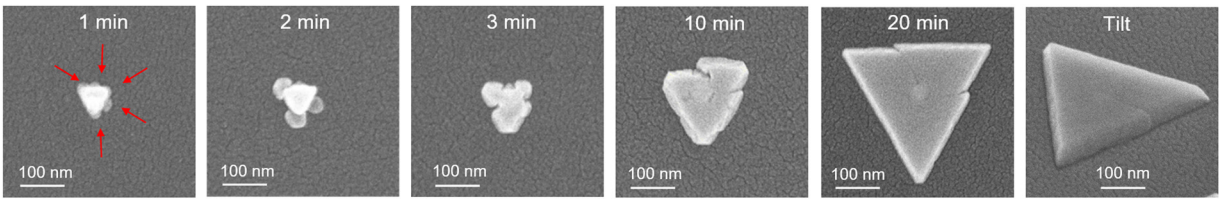

Fig. 4 SEM images showing a time sequence in the nanotriangle synthesis that leads to the formation of substrate-based Ag nanotriangles. The red arrows show the beginnings of planar Ag growth.

nanoplates derived from seeds produced in the same manner in that growth fronts emanate uniformly from the seed perimeter right from the onset of the reaction.[68]

Fig. 5(a) shows an AFM topographical image of an arrayed region showing a substantial size and shape distribution. Despite the nonuniformity, a line scan across the six nanoplates reveals a near-constant nanoplate height of 48 nm (Fig. 5(b)), a value that is consistent with the initial height of the Au seed. A close examination of a triangular nanoplate, exhibiting both crack (Fig. 5(c)) and void (Fig. 5(d)) surface features, shows a crack width of 24 nm where the value does not change appreciably along its length. It is also apparent that the crack extends down the side of the structures and appears to be highly disruptive to the formation of a well-formed nanotriangle vertex. With the understanding that the nanotriangle grows laterally, the crack can be followed back to its origin along a straight-line path that suddenly veers toward the seed, travels along its perimeter, and then terminates at a void. The width of the void is approximately the same as the crack width. The remainder of the seed perimeter is outlined by a shallow indentation. Hexagonal nanoplates also show crack and void features displaying similar tendencies where it is more prevalent to have multiple cracks on the same structure (Fig. S9, ESI†). With voids and cracks originating near the seed, this data points toward less-than-optimal early-stage heterogeneous nucleation processes where crack propagation ultimately becomes more favorable than the seamless merger of growth fronts.

Nanotriangle synthesis characterization was also carried out by spectroscopic means whereby a time progression of the extinction spectra was measured as a sample was periodically removed from the growth solution, cleaned and dried, characterized, and then reinserted back into the growth solution where its growth was allowed to continue. Although such a procedure comes with the inherent risk of not truly representing the growth sequence, it is noted that the final product did not differ significantly from identically produced samples where the growth was uninterrupted. Fig. 6(a) shows the extinction spectra obtained over a 35 min growth duration. It reveals a progression

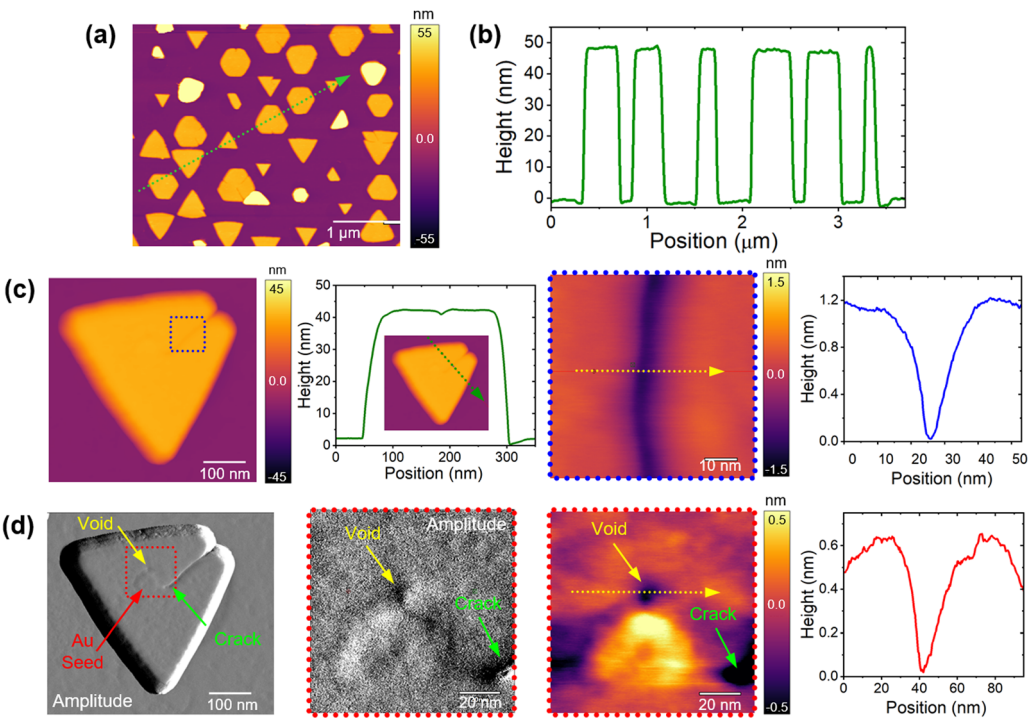

Fig. 5 (a) Topographic AFM image and (b) the associated line scan that reveals nanoplate height uniformity. Characterization of a single triangular nanoplate showing (c) crack- and (d) void-like features.

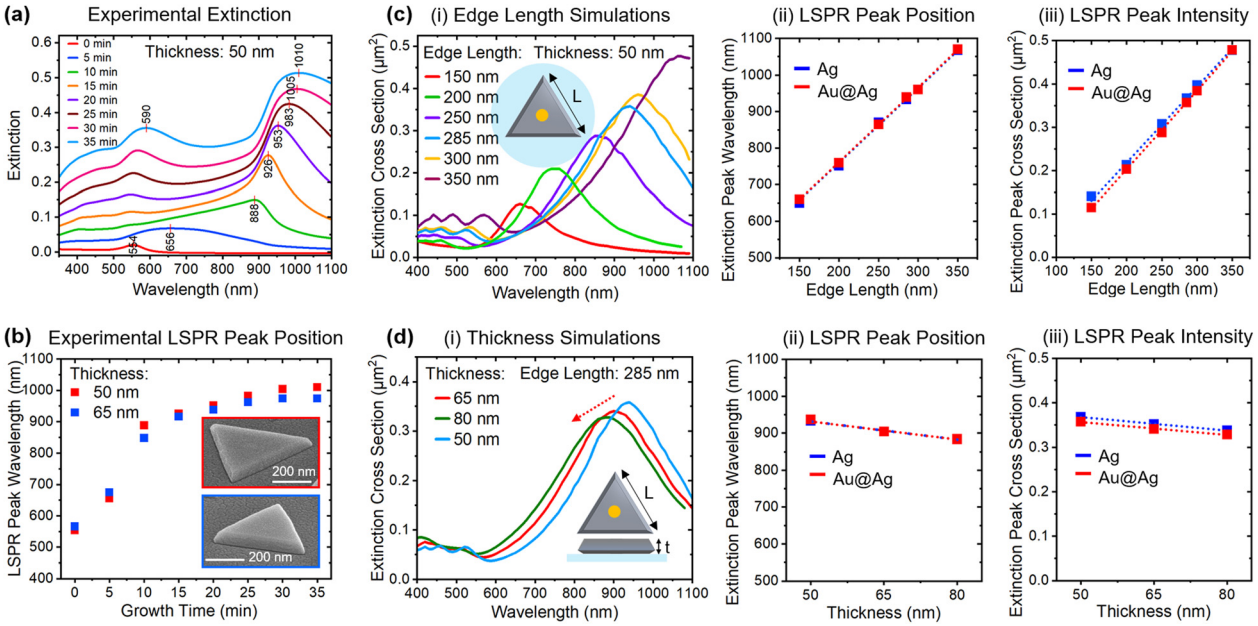

Fig. 6 (a) Time-dependent extinction spectra for a nanotriangle synthesis with a 35 min duration and the (b) associated time dependency of the LSPR peak wavelength. (c) Simulations of the (i) extinction cross section spectra for Ag nanotriangles with centrally located Au seed where the edge length is varied from 150 to 350 nm along with the extracted edge length dependencies on the (ii) LSPR peak wavelength and (iii) LSPR cross section. (d) Simulated extinction spectra as a function of nanotriangle thickness performed at constant edge length along with the analogous dependencies. For each of the dependencies shown in (c) and (d), a comparison is shown between that obtained for pure Ag nanotriangles (blue Ag curve) and identically sized Ag nanotriangles with a centrally located Au seed having a diameter of 75 nm (red Au@Ag curve).

that sees the emergence of an in-plane dipole plasmon resonance that red shifts and strengthens from the 554 nm resonance of the Au seed to the 1010 nm value expressed by the Ag nanotriangles. Fig. 6(b) shows the time-dependent variation to the dipole resonance wavelength along with those obtained for a nanotriangle where the seed thickness was increased from 50 to 65 nm (Fig. S10 (ESI†) provides the extinction spectra for the 65 nm thick sample). Despite the difference, both samples show a similar response whereby there exists a rapid increase followed by slow rise after 30 min. The rapid rise, which is accompanied by a transition from a rather broad peak to a well-defined peak occurring between 5 and 15 min, marks the transition from where the nanotriangles grow as disconnected segments to ones where they merge and assume a faceted morphology. Further red shifts are associated with increases to the nanotriangle edge length. The second resonance, which appears at 590 nm after 15 min, is assigned to the nanostructures that lack planar geometries (see Fig. 3(b)–(d)).

To gain further insights into these spectroscopic results, numerical simulations of the extinction cross section were performed where the Ag nanotriangle edge length and thickness were systemically varied. The simulations, while analogous to those obtained for colloidal structures,[69] take into account the considerably thicker nanotriangle widths obtained when using substrate-based seeds, the presence of a central Au seed, and the dielectric environment imposed by the sapphire substrate. These results should, however, be viewed with the caveat that they do not account for the observed segmented growth nor the fact that experimental results arise from a population of nanostructures with variations in both size and shape. Notwithstanding, the correspondence between the experimental and simulated spectra is considerable. Fig. 6(c) shows the extinction cross section spectra obtained as a function of nanotriangle edge length along with the extracted edge length dependencies of the extinction peak wavelength and extinction peak cross section for the dipole resonance. The data reveals that the dipole peak position for the Au@Ag nanotriangles varies linearly with edge length and, hence, provides a measure of the nanotriangle growth rate. The implication of this result, when compared to the experimental data shown in Fig. 6(b), is that the nanotriangle edge length increases in a near-linear manner for times between 10 and 25 min, after which the growth stagnates. This conclusion is consistent with SEM results that show few changes for extended growth times. Fig. 6(d) shows simulations where the nanotriangle thickness is varied from 35 to 80 nm as the edge length is held at a constant value of 285 nm. The results indicate that an increased plate thickness gives rise to a blue shift, a result that is consistent with prior work.[70] The degree of blue shift is consistent with the experimental results shown in Fig. 6(b). Simulations were also used to gauge the influence of the Au seed upon the extinction cross section. It is determined that its substitution for a Ag seed results in similar extinction spectra (Fig. S11, ESI†) for the seed and nanotriangle sizes simulated where the edge length and thickness dependencies on the dipole resonance position and extinction cross section follow near-identical trendlines for edge lengths above 150 nm (Fig. 6(c) and (d)).

Discussion

Given that the substrate-based synthesis forwarded in this work was adapted from a colloidal nanotriangle synthesis,[23] it is instructive to have an understanding of the commonalities and differences. Both syntheses are similar in that they invoke a two-stage protocol where seed preparation is distinct from nanotriangle syntheses. The Gao protocol uses Ag seeds that are derived from a separate colloidal synthesis[29] that gives rise to 5 nm thick triangular nanoplates with edge lengths of 30 nm and is, hence, enlarging nanostructures that already express the nanotriangle geometry. In sharp contrast, the seeds used in the current study are substrate-immobilized, composed of Au, and are near-hemispherical in shape with diameters in excess of 60 nm. The colloidal synthesis proceeds in a highly ordered manner that sees the triangular seeds uniformly enlarged whereas the substrate-based seeds show a somewhat disorganized nucleation process where the heterogeneous nucleation of Ag often occurs from multiple sites at the perimeter of a seed that is considerably larger than those typically used to initiate planar growth modes. As growth proceeds, order is partially restored as the various Ag domains grow and merge but defects remain in the form of voids at the seed perimeter and as crack-like features along the surface of the plate. The fact that these defects do not fully heal as growth continues is somewhat perplexing given that the seed imparts the same crystallographic character onto the various domains. It should, however, be recognized that the intersection of planar growth fronts supporting capping agents is neither a well-studied nor understood phenomena. Another significant difference in plate growth, which is not well-understood, is that the substrate-based synthesis sees the nanoplate growth essentially halt after 20 min whereas the colloidal synthesis has demonstrated edge-lengths as large as 1.5 μm. It is unlikely that this stagnation originates from a diminishing supply of reactants since they are supplied well in excess of what is needed to coat the entire substrate surface. Possible explanations for this stagnation include the oxidative etching of the side-facets coming into equilibrium with the deposition rate or the healing or poisoning of the stacking fault defects needed to support planar growth.

Even though these results represent a breakthrough in substrate-based Ag nanotriangle synthesis, the structures produced have deficiencies where most stem from seed inadequacies or nonuniform early-stage heterogeneous nucleation of Ag onto the Au seed. Further improvements in the seed fabrication process are, hence, needed to increase the yield of Au seeds with the desired crystallographic orientation and stacking fault defects. Improvements to the nanotriangle syntheses that support size and shape uniformity, and which eliminate the crack-like features visible on the planar surfaces, are also required. Moreover, these nanotriangles, like all Ag nanostructures, have plasmonic properties that are degraded upon prolonged exposure to air and show poor chemical stability in aqueous environments. It should, however, be noted that it is highly likely that these substrate-based nanotriangles are amenable to remedies directed toward mitigating these environmental sensitivities. The application of a protective ultrathin oxide coating can, for example, negate these environmental factors by providing a conformal passivating layer[71,72] while simultaneously providing functionality in applications such as shell-isolated nanoparticle-enhanced Raman spectroscopy (SHINERS) and plasmonic enhanced fluorescence.[73] The deposition of ultrathin Au layers over Ag nanostructures have also proved effective in enhancing the stability of Ag nanostructures while maintaining a plasmonic response that is dominated by the Ag component.[74,75] Additional opportunities should also arise by using these nanotriangles as sacrificial templates in galvanic replacement reactions or as a substructure in the creation of more sophisticated nanomaterials. With such post-synthesis transformations having already been demonstrated on colloidal nanotriangles, there exists a knowledge-base from which to draw on that has seen the formation of nanorings,[76] multimetallic alloys,[77] core–shell structures,[59,75] and porous nanoplates.[78] There is also the potential for extending the capabilities already demonstrated for substrate-based Au nanoplates to Ag, including the formation of nanoplates with variable shapes,[9,79] forming a hot spot in the nanogap formed between the tips of two adjacent nanotriangles,[80] and manipulating planar growth modes to realize chiral geometries.[68] All told, there exists a host of opportunities for realizing an expanded set of substrate-based structures that take advantage of both the plasmonic and chemical properties of Ag nanotriangles.

Conclusions

A first-of-its-kind substrate-based seed-mediated Ag nanoplate synthesis has been demonstrated where controls are put in place that regulate the position and orientation of the structures. The methods forwarded utilize the heteroepitaxial relationship between the substrate and Au seeds to set the seed orientation relative to the substrate and preferentially induce the symmetry-breaking stacking faults defects needed to support planar growth trajectories along the surface of the substrate. With these seed structures in place, nanoplate synthesis proceeds through the heteroepitaxial deposition of Ag onto the Au seed using suitably chosen reagents that ensure Ag^+ reduction, (111) capping, and the relatively slow kinetics needed to promote the nanoplate geometry. Taken together, the work adds another key building-block to the architecturally diverse library of nanostructures formed directly on substrate surfaces.

Experimental section

Chemicals and materials

Sapphire wafers (diameter = 100 mm, thickness = 0.65 mm, two-side polished) sourced from MTI Corporation were diced into 10 mm × 10.5 mm substrates. Au and Sb sputter deposition targets were cut from a 0.5 mm thick foil (99.9985% purity, Alfa Aesar) and 19 mm rod (99.999%, ESPI Metals), respectively. Seed assembly was carried out under an inert gas flow of ultrahigh purity Ar (Airgas). The nanoimprint lithography

process utilized a (i) bilayer resist composed of polydimethylglutarimide (PMGI SF 3S, Kayaku Advanced Materials) and mr-I 7030R (Micro Resist Technology), (ii) CD-26 developer diluted to 40% with H_2O, and (iii) 1,3-dioxolane solvent (EBR-PG). Stamps were obtained from LightSmyth Technologies and coated with a trichloro(1*H*,2*H*,2*H*-perfluorooctyl)silane (MilliporeSigma) anti-sticking layer. The reagents used in Ag nanotriangle synthesis are silver nitrate (Ward's Science), trisodium citrate dihydrate (Alfa Aesar), L-ascorbic acid (Macron Fine Chemicals), and acetonitrile (BDH Chemicals). Deionized (DI) H_2O with a resistivity of 18.2 MΩ cm was used in the preparation of all aqueous solutions.

Au seed fabrication

Periodic arrays of single-crystal Au seeds lined with stacking faults were fabricated using a slightly modified version of the procedures described in a prior report.[57] The key difference is that a bilayer resist is applied to the substrate instead of a single-layer resist whereby the topmost layer conforms to the stamp features while the bottom layer is chemically removed with a developer. The imprinting process, which occurs at 140 °C, embosses the uppermost resist with a stamp displaying a hexagonal array of cylinders (diameter = 240 nm, center-to-center distance = 600 nm, height = 350 nm, area = 8 mm × 8.3 mm). Reactive ion and chemical etchants are then sequentially applied to these resists where conditions are optimized to (i) expose the substrate surface at the imprinted sites and (ii) slightly undercut the topmost resist. Sb and Au layers are sputter deposited over the entire surface to thicknesses of 20 and 1.5 nm, respectively. This is followed by a lift-off procedure that leaves an array of Au-topped Sb disks where the undercut of the resist facilitates a crisp breakage point between the disks and unwanted material deposited on the sidewalls of the imprinted cylinders. Heating these structures to 1010 °C in flowing Ar results in assembly and crystallization of the Au seeds as the Sb is lost to sublimation. The so-formed arrays are typically cut into smaller pieces for use in multiple experiments. Additional details regarding array formation and the assembly process can be found elsewhere.[57,61,62]

Ag nanoplate synthesis

The Ag nanotriangle synthesis was adapted from the Gao protocol[23] where changes to the reagent concentrations and growth temperature have been made. Standard syntheses were carried out at room temperature under ambient lighting in a 30 mL Pyrex beaker containing a 1 cm Teflon stir bar rotating at 600 rpm. The synthesis proceeded by adding acetonitrile (10 mL), ascorbic acid (150 μL, 190 mM), and Na_3CA (100 μL, 50 mM) to 17 mL of DI H_2O. Once these reagents became thoroughly mixed, a substrate with a Au seed array was placed faceup at the bottom of the beaker where best efforts were made to have consistent placement from synthesis-to-synthesis so that a similar flow pattern would be realized. The synthesis is initiated through the rapid injection of $AgNO_3$ (120 μL, 50 mM) and allowed to continue for a duration that typically lasted 20 min. The reaction is terminated by retrieving the substrate from the growth solution with Teflon-coated tweezers, rinsing it in DI H_2O, and drying under a N_2 gas flow. Maintaining syntheses without the occurrence of a Ag colloid required that the beakers used in successive synthesis be thoroughly cleaned in *aqua regia* (Hazard: *aqua regia* is highly toxic and corrosive), swabbed, exposed to boiling DI H_2O, and rinsed in ethanol.

Simulations

Triangular nanostructures with various configurations and aspect ratios were formed using Crystal Creator,[81] a freely available crystal shape modeling tool that was modified to support the Winterbottom Wulff construction. Optical extinction spectra were obtained numerically in the discrete dipole approximation (DDA) using DDSCAT.[82] Each of the targeted shapes were modeled as a twinned nanotriangle resting on a 20 nm thick substrate that extends at least 40 nm from the edges and corners of the nanotriangle. The targeted systems had on the order of 10^5 dipoles with an interdipole distance of 3 nm. The refractive index of the surrounding ambient was set to 1. The wavelength-dependent refractive index of metallic Ag and Au were taken from Johnson and Christy[83] and that of the sapphire from Palik.[84] All calculations were carried out using orthogonally polarized light travelling perpendicular to the substrate. Extinction cross sections were calculated as $Q_{ext} \times \pi a_{eff}^2$, where Q_{ext} is the extinction efficiency given by DDSCAT and a_{eff} is the radius of an equivolume sphere.

Instrumentation

SEM imaging and elemental analysis were carried out using a Helios G4 Ux SEM/FIB workstation (FEI). AFM data were acquired with a Cypher ES AFM (Oxford Instruments). Spectroscopic characterization utilized a JASCO V-730 UV-Visible Spectrophotometer. A home-built imprinter[61] was used in the nanoimprint lithography process along with a SAMCO RIE-1C reactive ion etcher. Sputter depositions were carried out in a model 681 Gatan high resolution ion beam coater. A Lindberg Blue M furnace equipped with a quartz tube and an Ar gas handling system was used for seed assembly processes.

Conflicts of interest

There are no conflicts to declare.

Acknowledgements

This work was supported by the National Science Foundation, Division of Chemistry, Macromolecular, Supramolecular, and Nanochemistry (MSN) Program under Grant No. CHE-2107728 to S. N. It has also benefited from the facilities available through the Notre Dame Integrated Imaging Facility (NDIIF). E. R. acknowledges support from the EU Framework Programme for Research and Innovation Horizon 2020 (ERC Starting Grant SPECs 804523).

Notes and references

1 Q. N. Nguyen, C. Wang, Y. Shang, A. Janssen and Y. Xia, Colloidal synthesis of metal nanocrystals: From asymmetrical growth to symmetry breaking, *Chem. Rev.*, 2023, **123**, 3693–3760.

2 T. Yang, Y. Shi, A. Janssen and Y. Xia, Surface capping agents and their roles in shape controlled synthesis of colloidal metal nanocrystals, *Angew. Chem., Int. Ed.*, 2020, **59**, 15378–15401.

3 L. Scarabelli, M. Sun, X. Zhuo, S. Yoo, J. E. Millstone, M. R. Jones and L. M. Liz-Marzán, Plate-like colloidal metal nanoparticles, *Chem. Rev.*, 2023, **123**, 3493–3542.

4 R. D. Neal, R. A. Hughes, A. S. Preston, S. D. Golze, T. D. Demille and S. Neretina, Substrate-immobilized noble metal nanoplates: A review of their synthesis, assembly, and application, *J. Mater. Chem. C*, 2021, **9**, 12974–13012.

5 S. Yu, C. Zhang and H. Yang, Two-dimensional metal nanostructures: From theoretical understanding to experiment, *Chem. Rev.*, 2023, **123**(7), 3443–3492.

6 Y. Chen, Z. Fan, Z. Zhang, W. Niu, C. Li, N. Yang, B. Chen and H. Zhang, Two-dimensional metal nanomaterials: Synthesis, properties, and applications, *Chem. Rev.*, 2018, **118**, 6409–6455.

7 J. E. Millstone, S. J. Hurst, G. S. Métraux, J. I. Cutler and C. A. Mirkin, Colloidal gold and silver triangular nanoprisms, *Small*, 2009, **5**, 646–664.

8 Q. Zhang, Y. Hu, S. Guo, J. Goebl and Y. Yin, Seeded growth of uniform Ag nanoplates with high aspect ratio and widely tunable surface plasmon bands, *Nano Lett.*, 2010, **10**, 5037–5042.

9 R. D. Neal, Z. R. Lawson, W. J. Tuff, K. Xu, V. Kumar, M. T. Korsa, M. Zhukovskyi, M. R. Rosenberger, J. Adam, J. A. Hatchel, J. P. Camden, R. A. Hughes and S. Neretina, Large-area periodic arrays of atomically flat single-crystal gold nanotriangles formed directly on substrate surfaces, *Small*, 2022, **18**, 2205780.

10 E. Hao and G. C. Schatz, Electromagnetic fields around silver nanoparticles and dimers, *J. Chem. Phys.*, 2004, **120**, 357–366.

11 M. Rycenga, C. M. Cobley, J. Zeng, W. Li, C. H. Moran, Q. Zhang, D. Qin and Y. Xia, Controlling the synthesis and assembly of silver nanostructures for plasmonic applications, *Chem. Rev.*, 2011, **111**, 3669–3712.

12 J. Otsuki, K. Sugawa and S. Jin, Plasmonic triangular nanoprism sensors, *Mater. Adv.*, 2021, **2**, 32–46.

13 T. Tan, S. Zhang, J. Wang, Y. Zheng, H. Lai, J. Liu, F. Qin and C. Wang, Resolving the stacking fault structure of silver nanoplates, *Nanoscale*, 2021, **13**, 195–205.

14 D. Aherne, D. M. Ledwith, M. Gara and J. M. Kelly, Optical properties and growth aspects of silver nanoprisms produced by a highly reproducible and rapid synthesis at room temperature, *Adv. Funct. Mater.*, 2008, **18**, 2005–2016.

15 V. Germain, J. Li, D. Ingert, Z. L. Wang and M. P. Pileni, Stacking faults in formation of silver nanodisks, *J. Phys. Chem. B*, 2003, **107**, 8717–8720.

16 R. Jagannathan, R. V. Mehta, J. A. Timmons and D. L. Black, Anisotropic growth of twinned cubic crystals, *Phys. Rev. B: Condens. Matter Mater. Phys.*, 1993, **48**, 261–265.

17 H. Xu and B. J. Wiley, The roles of citrate and defects in the anisotropic growth of Ag nanostructures, *Chem. Mater.*, 2021, **33**, 8301–8311.

18 R. Jin, Y. Cao, C. A. Mirkin, K. L. Kelly, G. C. Schatz and J. G. Zheng, Photo-induced conversion of silver nanospheres to nanoprisms, *Science*, 2001, **294**, 1901–1903.

19 H. Yu, Q. Zhang, H. Liu, M. Dahl, J. B. Joo, N. Li, L. Wang and Y. Yin, Thermal synthesis of silver nanoplates revisited: A modified photochemical process, *ACS Nano*, 2014, **8**, 10252–10261.

20 N. Li, Q. Zhang, S. Quinlivan, J. Goebl, Y. Gan and Y. Yin, H_2O_2-aided seed-mediated synthesis of silver nanoplates with improved yield and efficiency, *ChemPhysChem*, 2012, **13**, 2526–2530.

21 M. R. Langille, M. L. Personick and C. A. Mirkin, Plasmon-mediated syntheses of metallic nanostructures, *Angew. Chem., Int. Ed.*, 2013, **52**, 13910–13940.

22 B. Xue, D. Wang, J. Zuo, X. Kong, Y. Zhang, X. Liu, L. Tu, Y. Chang, C. Li, F. Wu, Q. Zeng, H. Zhao, H. Zhao and H. Zhang, Towards high quality triangular silver nanoprisms: Improved synthesis, six-tip based hot spots and ultra-high local surface plasmon resonance sensitivity, *Nanoscale*, 2015, **7**, 8048–8057.

23 X. Liu, L. Li, Y. Yang, Y. Yin and C. Gao, One-step growth of triangular silver nanoplates with predictable sizes on a large scale, *Nanoscale*, 2014, **6**, 4513–4516.

24 G. S. Métraux and C. A. Mirkin, Rapid thermal synthesis of silver nanoprisms with chemically tailorable thickness, *Adv. Mater.*, 2005, **17**, 412–414.

25 I. Washio, Y. Xiong, Y. Yin and Y. Xia, Reduction by the end groups of poly(vinyl pyrrolidone): A new and versatile route to the kinetically controlled synthesis of Ag triangular nanoplates, *Adv. Mater.*, 2006, **18**, 1745–1749.

26 Q. Zhang, Y. Yang, J. Li, R. Iurilli, S. Xie and D. Qin, Citrate-free synthesis of silver nanoplates and the mechanistic study, *ACS Appl. Mater. Interfaces*, 2013, **5**, 6333–6345.

27 D. S. Kilin, O. V. Prezhdo and Y. Xia, Shape-controlled synthesis of silver nanoparticles: Ab initio study of preferential surface coordination with citric acid, *Chem. Phys. Lett.*, 2008, **458**, 113–116.

28 Z. Tang, Q. Zhang, Y. Yin and C. E. A. Chang, Facet selectivity of ligands on silver nanoplates: Molecular mechanics study, *J. Phys. Chem. C*, 2014, **118**, 21589–21598.

29 Q. Zhang, N. Li, J. Goeble, Z. Lu and Y. A. Yin, Systematic study of the synthesis of silver nanoplates: Is citrate a "magic" reagent?, *J. Am. Chem. Soc.*, 2011, **133**, 18931–18939.

30 Y. M. Park, B. G. Lee, J.-I. Weon and M. H. Kim, One-step synthesis of silver nanoplates with high aspect ratios: Using coordination of silver ions to enhance lateral growth, *RSC Adv.*, 2016, **6**, 95768–95773.

31 R. Mravljak and A. Podgornik, Simple and tailorable synthesis of silver nanoplates in gram quantities, *ACS Omega*, 2023, **8**, 2760–2772.

32 J. Zeng, X. Xia, M. Rycenga, P. Henneghan, Q. Li and Y. Xia, Successive deposition of silver on silver nanoplates: Lateral versus vertical growth, *Angew. Chem., Int. Ed.*, 2011, **50**, 244–249.

33 C. N. Grabilla, D. Freppona, M. Hettingera and S. M. Kuebler, Nanoscale morphology of electrolessly deposited silver metal, *Appl. Surf. Sci.*, 2019, **466**, 230–243.
34 F. Muench, R. Popovitz-Biro, T. Bendikov, Y. Feldman, B. Hecker, M. Oezaslan, I. Rubinstein and A. Vaskevich, Nucleation-controlled solution deposition of silver nanoplate architectures for facile derivatization and catalytic applications, *Adv. Mater.*, 2018, **30**, 1805179.
35 N. A. Bakar, J. G. Shapter, M. M. Salleh and A. A. Umar, Self-assembly of high density of triangular silver nanoplate films promoted by 3-aminopropyltrimethoxysilane, *Appl. Sci.*, 2015, **5**, 209–221.
36 Y. K. Kim and D. H. Min, Surface confined successive growth of silver nanoplates on a solid substrate with tunable surface plasmon resonance, *RSC Adv.*, 2014, **4**, 6950–6956.
37 H. Jia, J. Zeng, J. An, W. Song, W. Xu and B. Zhao, Preparation of triangular and hexagonal silver nanoplates on the surface of quartz substrate, *Thin Solid Films*, 2008, **516**, 5004–5009.
38 K. Aslan, J. R. Lakowicz and C. D. Geddes, Rapid deposition of triangular silver nanoplates on planar surfaces: Application to metal-enhanced fluorescence, *J. Phys. Chem. B*, 2005, **109**, 6247–6251.
39 Q. Wu, P. Diao, J. Sun, T. Jin, D. Xu and M. Xiang, Electrodeposition of vertically aligned silver nanoplate arrays on indium tin oxide substrates, *J. Phys. Chem. C*, 2015, **119**, 20709–20720.
40 S. Yang, D. Slotcavage, J. D. Mai, F. Guo, S. Li, Y. Zhao, Y. Lei, C. E. Cameron and T. J. Huang, Electrochemically created highly surface roughened Ag nanoplate arrays for SERS biosensing applications, *J. Mater. Chem. C*, 2014, **2**, 8350–8356.
41 S. H. Park, J. G. Son, T. G. Lee, H. M. Park and J. Y. Song, One-step large-scale synthesis of micrometer-sized silver nanosheets by a template-free electrochemical method, *Nanoscale Res. Lett.*, 2013, **8**, 1–6.
42 G. Liu, W. Cai, L. Kong, G. Duan and F. Lü, Vertically Cross-linking silver nanoplate arrays with controllable density based on seed-assisted electrochemical growth and their structurally enhanced SERS activity, *J. Mater. Chem.*, 2010, **20**, 767–772.
43 G. Liu, W. Cai and C. Liang, Trapeziform Ag nanosheet arrays induced by electrochemical deposition on Au-coated substrate, *Cryst. Growth Des.*, 2008, **8**, 2748–2752.
44 T.-J. Wang, H. W. Chang, Y.-Y. Wang, H. A. Chi and J.-S. Chen, One-step surfactant-free photoreduction synthesis of single-crystal silver triangular nanoprisms by surface modified chemically patterned ferroelectric crystals for SERS application, *Appl. Surf. Sci.*, 2023, **623**, 157114.
45 Y. Wang, C. Wang, Y. Zhang, J. Wang and L. Wang, Preparation of silver nanosheet-assembled film as a surface-enhanced Raman scattering substrate, *Rev. Anal. Chem.*, 2022, **41**, 256–266.
46 Y. Sun, Metal nanoplates on semiconductor substrates, *Adv. Funct. Mater.*, 2010, **20**, 3646–3657.
47 Y. Sun, Synthesis of Ag nanoplates on GaAs wafers: Evidence for growth mechanism, *J. Phys. Chem. C*, 2010, **114**, 857–863.
48 G. A. Vinnacombe-Wilson, Y. Conti, A. Stefancu, P. S. Weiss, E. Corte and L. Scarabelli, Direct bottom-up in situ growth: A paradigm shift for studies in wet-chemical synthesis of gold nanoparticles, *Chem. Rev.*, 2023, **123**, 8488–8529.
49 H. Zhang, C. Kinnear and P. Mulvaney, Fabrication of single-nanocrystal arrays, *Adv. Mater.*, 2020, **32**, 1904551.
50 S. V. Grayli, X. Zhang, F. C. MacNab, S. Kamal, D. Star and G. W. Leach, Scalable, green fabrication of single-crystal noble metal films and nanostructures for low-loss nanotechnology applications, *ACS Nano*, 2020, **14**, 7581–7592.
51 H. Zhang, Y. Liu, M. F. S. Shahidan, C. Kinnear, F. Maasoumi, J. Cadusch, E. M. Akinoglu, T. D. James, A. Widmer-Cooper, A. Roberts and P. Mulvaney, Direct assembly of vertically oriented, gold nanorod arrays, *Adv. Funct. Mater.*, 2021, **31**, 2006753.
52 S. Denga, R. Lib, J. E. Parka, J. Guanc, P. Chooa, J. Hua, P. J. M. Smeets and T. W. Odom, Ultranarrow plasmon resonances from annealed nanoparticle lattices, *Proc. Natl. Acad. Sci. U. S. A.*, 2020, **117**, 23380–23384.
53 G. A. Vinnacombe-Willson, J. K. Lee, N. Chiang, L. Scarabelli, S. Yue, R. Foley, I. Frost, P. S. Weiss and S. J. Jonas, Exploring the bottom-up growth of anisotropic gold nanoparticles from substrate-bound seeds in microfluidic reactors, *ACS Appl. Nano Mater.*, 2023, **6**, 6454–6460.
54 J. Jia, N. Metzkow, S.-M. Park, Y. L. Wu, A. D. Sample, B. Diloknawarit, I. Jung and T. W. Odom, Spike growth on patterned gold nanoparticle scaffolds, *Nano Lett.*, 2023, **23**, 11260–11265.
55 G. Liu, C. Zhang, J. Wu and C. A. Mirkin, Using scanning-probe block copolymer lithography and electron microscopy to track shape evolution in multimetallic nanoclusters, *ACS Nano*, 2015, **9**, 12137–12145.
56 M. Stefik, S. Guldin, S. Vignolini, U. Wiesner and U. Steiner, Block copolymer self-assembly for nanophotonics, *Chem. Soc. Rev.*, 2015, **44**, 5076–5091.
57 S. D. Golze, R. A. Hughes, S. Rouvimov, R. D. Neal, T. B. Demille and S. Neretina, Plasmon-mediated synthesis of periodic arrays of gold nanoplates using substrate-immobilized seeds lined with planar defects, *Nano Lett.*, 2019, **19**, 5653–5660.
58 Y. Xia, K. D. Gilroy, H. Peng and X. Xia, Seed-mediated growth of colloidal metal nanocrystals, *Angew. Chem., Int. Ed.*, 2017, **56**, 60–95.
59 C. Xue, J. E. Millstone, S. Li and C. A. Mirkin, Plasmon-driven synthesis of triangular core-shell nanoprisms from gold seeds, *Angew. Chem., Int. Ed.*, 2007, **46**, 8436–8439.
60 J. Goebl, Q. Zhang, L. He and Y. Yin, Monitoring the shape evolution of silver nanoplates: A marker study, *Angew. Chem., Int. Ed.*, 2012, **124**, 567–570.
61 E. Menumerov, S. D. Golze, R. A. Hughes and S. Neretina, Arrays of highly complex noble metal nanostructures using nanoimprint lithography in combination with liquid-phase epitaxy, *Nanoscale*, 2018, **10**, 18186–18194.
62 P. Farzinpour, A. Sundar, K. D. Gilroy, Z. E. Eskin, R. A. Hughes and S. Neretina, Dynamic templating: A large

area processing route for the assembly of periodic arrays of sub-micrometer and nanoscale structures, *Nanoscale*, 2013, **5**, 1929–1938.

63 S. D. Golze, R. A. Hughes, E. Menumerov, S. Rouvimov and S. Neretina, Synergistic roles of vapor- and liquid-phase epitaxy in the seed-mediated synthesis of substrate-based noble metal nanostructures, *Nanoscale*, 2021, **13**, 20225–20233.

64 C. R. Henry, Morphology of supported Nanoparticles, *Prog. Surf. Sci.*, 2015, **80**, 92–116.

65 A. S. Preston, R. A. Hughes, T. B. Demille, V. M. Rey Davila and S. Neretina, Dewetted nanostructures of gold, silver, copper, and palladium with enhanced faceting, *Acta Mater.*, 2019, **165**, 15–25.

66 M. Hajfathalian, K. D. Gilroy, R. A. Hughes and S. Neretina, Citrate-induced nanocubes: A re-examination of the role of citrate as a shape-directing capping agent for Ag-based nanostructures, *Small*, 2016, **12**, 3444–3452.

67 K. D. Gilroy, J. Puibasset, M. Vara and Y. Xia, On the Thermodynamics and experimental control of twinning in metal nanocrystals, *Angew. Chem., Int. Ed.*, 2017, **56**, 8647–8651.

68 S. D. Golze, S. Porcu, C. Zhu, E. Sutter, P. C. Ricci, E. C. Kinzel, R. A. Hughes and S. Neretina, Sequential symmetry-breaking events as a synthetic pathway for chiral gold nanostructures with spiral geometries, *Nano Lett.*, 2021, **21**, 2919–2925.

69 M. G. Blaber, A.-I. Henry, J. M. Bingham, G. C. Schatz and R. P. Van Duyne, LSPR imaging of silver triangular nanoprisms: Correlating scattering with structure using electrodynamics for plasmon lifetime analysis, *J. Phys. Chem. C*, 2012, **116**, 393–403.

70 Y. B. Zheng, B. K. Juluri, X. Mao, T. R. Walker and T. J. Huang, Systematic investigation of localized surface plasmon resonance of long-range ordered Au nanodisk arrays, *J. Appl. Phys.*, 2008, **103**, 014308.

71 A. S. Preston, R. A. Hughes, N. L. Dominique, J. P. Camden and S. Neretina, Stabilization of plasmonic silver nanostructures with ultrathin oxide coatings formed using atomic layer deposition, *J. Phys. Chem. C*, 2021, **125**, 17212–17220.

72 A. S. Preston, R. A. Hughes, T. B. Demille and S. Neretina, Plasmonics under attack: Protecting copper nanostructures from harsh environments, *Chem. Mater.*, 2020, **32**, 6788–6799.

73 C. Li and Y. Jin, Shell-isolated plasmonic nanostructures for biosensing, catalysis, and advanced nanoelectronics, *Adv. Funct. Mater.*, 2021, **31**, 2008031.

74 Y. Yang, J. Liu, Z. W. Fu and D. Qin, Galvanic replacement-free deposition of Au on Ag for core-shell nanocubes with enhanced chemical stability and SERS activity, *J. Am. Chem. Soc.*, 2014, **136**, 8153–8156.

75 H. Liu, T. Liu, L. Zhang, L. Han, C. Gao and Y. Yin, Etching-free epitaxial growth of gold on silver nanostructures for high chemical stability and plasmonic activity, *Adv. Funct. Mater.*, 2015, **25**, 5435–5443.

76 H. Qian, M. Xu, X. Li, M. Ji, L. Cheng, A. Shoaib, J. Liu, L. Jiang, H. Zhu and J. Zhang, Surface micro/nanostructure evolution of Au–Ag Alloy nanoplates: Synthesis, simulation, plasmonic photothermal and surface-enhanced Raman scattering applications, *Nano Res.*, 2016, **9**, 876–885.

77 Y. Q. Zheng, X. P. Wang, Y. H. Kong and Y. Y. Ma, Two-dimensional multimetallic alloy nanocrystals: Recent progress and challenges, *CrystEngComm*, 2021, **23**, 6454–6469.

78 X. Wei, Q. Fan, H. Liu, Y. Bai, L. Zhang, H. Zheng, Y. Yin and C. Gao, Holey Au–Ag alloy nanoplates with built-in hotspots for surface-enhanced Raman scattering, *Nanoscale*, 2016, **8**, 15689–15695.

79 T. B. Demille, R. D. Neal, A. S. Preston, Z. Liang, A. G. Oliver, R. A. Hughes and S. Neretina, Epitaxially aligned single-crystal gold nanoplates formed in large-area arrays at high yield, *Nano Res.*, 2022, **15**, 296–303.

80 Y. Zhou, X. Zhou, D. J. Park, K. Torabi, K. A. Brown, M. R. Jones, C. Zhang, G. C. Schatz and C. A. Mirkin, Shape-selective deposition and assembly of anisotropic nanoparticles, *Nano Lett.*, 2014, **14**, 2157–2161.

81 C. Boukouvala and E. Ridge, Wulff-based approach to modeling the plasmonic response of single crystal, twinned, and core–shell nanoparticles, *J. Phys. Chem. C*, 2019, **123**, 25501–25508.

82 B. T. Draine and P. J. Flatau, Discrete-dipole approximation for scattering calculations, *J. Opt. Soc. Am. A*, 1994, **11**, 1491–1499.

83 P. B. Johnson and R. W. Christy, Optical constants of the noble metals, *Phys. Rev. B: Solid State*, 1972, **6**, 4370–4379.

84 E. D. Palik, *Handbook of optical constants of solids*, Academic Press, San Diego, 1998.